Int. J. Heat Mass Transfer. Vol. 32, No. 1, pp. 47–68, 1989
Printed in Great Britain

0017–9310/89 $3.00 + 0.00

Solidification of an aqueous ammonium chloride solution in a rectangular cavity—I. Experimental study

M. S. CHRISTENSON and F. P. INCROPERA
Heat Transfer Laboratory, School of Mechanical Engineering, Purdue University, West Lafayette, IN 47907, U.S.A.

(*Received* 4 *March* 1988 *and in final form* 8 *June* 1988)

Abstract—An experimental study of solidification is performed for a binary NH_4Cl–H_2O solution in a rectangular cavity with varying initial concentration and thermal boundary conditions. Solutally driven flows are found to strongly influence solidification rates, localized remelting, and macroscopic solute redistribution. Control of these flows is effected through selection of the thermal conditions imposed on the solidification process.

1. INTRODUCTION

SINCE solidification is inherently characterized by thermal, and possibly solutal, gradients in the liquid, the presence of a body force, such as gravity, establishes natural convection flows which can strongly influence progression of the solidification process. In recent years, this influence has become more widely recognized, and related research has been stimulated by a broad range of engineering and geophysical phenomena. Engineering applications relate to the growth of pure crystals for the microelectronics industry [1], the development of latent heat of fusion thermal energy storage devices [2], the casting of pure and binary metals [3], and to welding and soldering processes [4]. Applications to geophysical phenomena relate, for example, to solidification in magma chambers [5] and icebergs [6].

The effect of natural convection on the solidification of pure substances has been studied extensively, and comprehensive reviews of the subject are available [7, 8]. In contrast, the solidification of multicomponent substances has received comparatively little attention. In such substances, convection may be driven by solutal, as well as thermal, buoyancy forces and may, for example, influence the homogeneity and crystal structure of alloyed metallic castings. It is well known that flow in the liquid regions of such castings greatly influences the quality of the final product [9, 10] and that knowledge of momentum, energy and species transfer due to natural convection in the melt is essential to maintaining satisfactory control over the casting process.

Fisher [3] has summarized the relationship between fluid flow in the melt and the process of macrosegregation, which refers to the large-scale separation of alloy components and is the major source of inhomogeneities in castings. As solidification of a binary mixture occurs, solute enrichment or depletion of the remaining liquid phase results from differences in the component solubilities in the solid and liquid phases. Solute enrichment or depletion of the liquid occurs in a two-phase, porous (mushy) region, while solutally and thermally induced buoyancy forces can drive the liquid through and from the mushy region. In this way alloy components may be redistributed into segregates, or regions that are rich/lean in a particular constituent.

Much of the experimental work performed to date has involved liquid metal alloys, such as Al–Cu and Sn–Pb systems, as well as transparent analogs such as NH_4Cl and Na_2CO_3 salt solutions. The experiments have typically involved solidification from vertical or horizontal surfaces characteristic of static and continuous casting processes. In an early work, Mehrabian *et al.* [10] studied macrosegregation in the unidirectional solidification of Al–Cu at a vertical wall. Temperature measurements were used to track the advancing solidification front, and macrosegregation was quantified from analysis of the final casting. Macrosegregation was attributed to gravity induced interdendritic flows. The same conclusion was reached by McDonald and Hunt [11] through flow visualization studies of solidification in an NH_4Cl–H_2O solution. Asai and Muchi [12] also performed flow visualization studies for a solidifying NH_4Cl–H_2O solution and revealed the influence of interdendritic flows on the formation of channel type segregates. Working with solidification of a Pb–Sn alloy from a vertical sidewall, Stewart and Weinberg [13] concluded from flow visualization (using radioactive tracers) that thermal convection was largely responsible for the liquidus interface shape and that the penetration of bulk liquid into the interdendritic regions was small. Other more recent qualitative studies in transparent analog castings have confirmed the role of convection in forming channel segregates [14] and equiaxed zones [15, 16].

Although past studies have done much to reveal the nature of macrosegregation and the columnar to

equiaxed transition in ingots, little has been done to determine temperature, velocity, and concentration fields within a solidifying binary mixture and to resolve, in detail, the effects of transport processes occurring during solidification. Szekely and Jassal [17] combined temperature and velocity measurements with photographic observations of a solidifying NH_4Cl–H_2O solution, and the appearance of double-diffusive convection effects, as described by Turner [18], were noted for the first time. Although the results provided tangible evidence of the importance of solutally driven interdendritic flows, concentration profile data were lacking and the analysis and discussion of transport processes were limited. In a more recent study of solidification for the Na_2CO_3–H_2O system [19], double-diffusive layering was observed to progress from the bottom of a rectangular cavity, as solidification was induced at one vertical wall and the opposing wall was heated. For the hypoeutectic conditions of the study (initial Na_2CO_3 composition less than the eutectic), rejection of the heavier Na_2CO_3 induced a stable vertical solute gradient in the melt. In the presence of a horizontal temperature gradient, a succession of horizontal double-diffusive convection layers was produced in the manner reported by Chen [20]. Also, for the NH_4Cl–H_2O system, temperature and concentration profiles have recently been measured and used with shadowgraphic observations to determine the effect of variations in initial concentration and wall temperature on double-diffusive layering [21].

The objective of the present study has been to perform temperature and concentration measurements, as well as flow visualization, for solidification of the NH_4Cl–H_2O system in a rectangular cavity. Solidification was induced at one of the vertical walls, while the opposite wall was either insulated or maintained at the initial (superheated) temperature of the solution. Experimental conditions extend well beyond those previously considered, and the results reveal many important features of the thermally and solutally driven flows. The contents of this paper are restricted to presentation and interpretation of the experimental results. In a companion paper [22], experimental results are compared with predictions based on a recently developed continuum model for solidification in binary mixtures [23].

2. EXPERIMENTAL PROCEDURES

A schematic of the test cell is shown in Fig. 1. The system consists of two copper heat exchangers for control of the sidewall thermal conditions, clear acrylic endwalls for visual access to the solidification process, and acrylic base and lid components to complete the enclosure. The cavity height and length were fixed at $H = 144$ mm and $L = 36$ mm, respectively, providing an aspect ratio of $A = 4$. The width of $2W = 200$ mm was sufficiently large to render three-dimensional (end) effects negligible. Fluid contact with the top surface was maintained throughout the experiments in order to eliminate thermo/diffusocapillary effects.

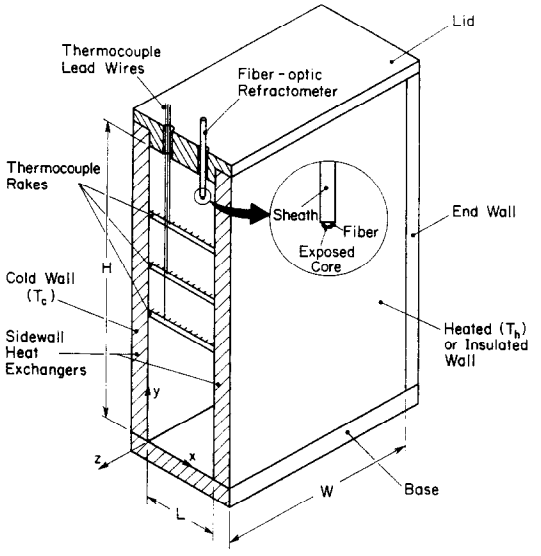

FIG. 1. Schematic of test cell sectioned at its midplane (as measured from the cold wall, rake thermocouple locations correspond to $x = 2.2$, 4.4, 6.6, 8.7, 10.9, 13.1, 15.3, 17.5, 21.8, 26.2, and 30.6 mm).

To effect thermal control over the system, the sidewall heat exchangers were each equipped with a single serpentine passage through which a working fluid could pass. Thermal conditions were set through two constant temperature baths. One bath (Neslab ULT-80DD) was operated with pure ethyl alcohol to maintain low temperature conditions ($-70°C < T_c < 0°C$), while a second bath (Lauda NBSD Ultra-Thermostat) was operated with water for high temperature conditions ($T_h = 40°C$). While solidification was induced at the cold wall ($x = 0$), the opposite wall ($x = L$) was either heated, to maintain it at the initial temperature of the solution, or insulated. The entire test cell was encased in 50.8 mm thick Styrofoam insulation to minimize heat transfer from the ambient during experimentation.

Temperature distributions in the test region were obtained by means of three horizontal rakes, each of which was installed at the midplane of the test section ($z = 0$ mm) and contained eleven copper–constantan thermocouple junctions. The rakes were positioned at three vertical locations within the cavity, corresponding to elevations of $y = 45$, 65, and 90 mm from the bottom. The spacing between thermocouple junctions was staggered, with more junctions installed near the cold wall where large temperature gradients were expected. With this arrangement, horizontal and vertical temperature distributions could be obtained as a function of time throughout the solidification process. Calibration of the thermocouples indicated

accuracy to within ± 0.05°C. The rakes were coated with an epoxy for protection from the corrosive NH_4Cl–H_2O environment. The time constant for an epoxy-coated thermocouple (70 ms) was much smaller than the time (~ 20 s) typically required for a 1°C temperature change within the system. Thermocouples installed in each heat exchanger plate were used to measure sidewall temperatures and to determine the extent of temperature variations across each plate (± 0.1°C).

The change in concentration over time at a single location within the cavity was determined using a recently developed miniature fiber-optic refractometer [24]. The refractometer consisted of a single, 0.5 mm diameter, plastic core, optical fiber bent into a U-shape and sheathed with stainless steel tubing (Fig. 1). At the tip of the U bend, the normal cladding of the fiber was removed in order to expose the actual core. As light traverses a sharp bend in the fiber, the amount that remains in the fiber (or conversely the amount that is lost through the bend) depends on the refractive index of the material to which the core of the fiber is exposed. By measuring the amount of light transmitted through the fiber, the refractive index of the surrounding medium can be determined. Since refractive index depends on the density of the medium, which in turn depends on the temperature and concentration, simultaneous measurement of the transmitted light and the local temperature will yield the local concentration.

A 5 mW He–Ne laser beam was used as the input to the refractometer, and the output was detected with a photodiode. The electric current output of the photodiode was transformed to a voltage which was measured using a digital voltmeter. Small random fluctuations inherent in the laser light source induced a measurement uncertainty of ± 3 mV.

Calibration of the refractometer probe was effected by measuring probe output (in volts) as a function of temperature for NH_4Cl–H_2O solutions of varying concentration. However, for the temperature range of interest in this study, variation of the probe output with temperature was small and well within accuracy limits of the device. Since the only detectable changes in probe output were due to variations in concentration, the probe could be used without a concurrent temperature measurement. With respect to concentration, the sensitivity of the refractometer was determined to be 6 mV/% change in concentration. Thus, in terms of concentration, the accuracy of the device was $\pm 0.5\%$.

The uncladded portion of the refractometer (the probe tip) was placed close to the top of the cavity, at x and y locations of 27 and 135 mm, respectively. This choice was motivated by the expectation that the largest concentration changes should occur in the upper region of the cavity [25] and by the fact that this region should be the last to solidify, thereby maximizing the time interval of the measurement process. Uncertainty in the placement of the probe was determined to be ± 0.5 mm in the x- and z-directions and ± 1.0 mm in the y-direction. The spatial resolution of the probe was approximately $0.5 \times 0.0 \times 1.0$ mm in the x-, y-, and z-directions, respectively.

The equilibrium phase diagram for aqueous ammonium chloride, which has a eutectic temperature and composition (NH_4Cl mass fraction) of $T_e = -15.4$°C and $f_e = 19.7\%$, respectively, is shown in Fig. 2. This solution was selected for several reasons which include: (1) its semitransparency, which facilitates flow visualization, (2) its similarity to liquid metal solidification in terms of dendritic growth of the solid phase, (3) the availability of thermophysical property data, which facilitates numerical simulation, and (4) the flexibility which it provides for experimenting over a wide range of conditions corresponding to thermal and solutal buoyancy forces of varying magnitude and direction. A major disadvantage of NH_4Cl–H_2O solutions is their extreme corrosiveness, which significantly reduces the life of test cell components and instrumentation.

To begin an experiment, a solution of the desired composition was prepared by mixing the corresponding amounts of ammonium chloride and water. The hot wall heat exchanger was set to the desired initial temperature ($T_h = 40$°C in all cases); the solution was poured; and the system was allowed to equilibrate. At $t = 0$, the cold wall was reduced to the desired temperature, while the opposite wall was either maintained at the initial temperature or insulated. As solidification commenced, temperature and concentration data were read and stored by a HP3054A data acquisition system. At selected times during the process, the insulation was removed from the surfaces at $z = \pm W$ and a photographic record was obtained. Two incandescent sources provided the necessary illumination from both the front and the back of the test cell.

The experiment was terminated when a steady-state condition was reached. With a heated wall at $x = L$, complete solidification did not occur and steady state was assumed to exist when none of the recorded tem-

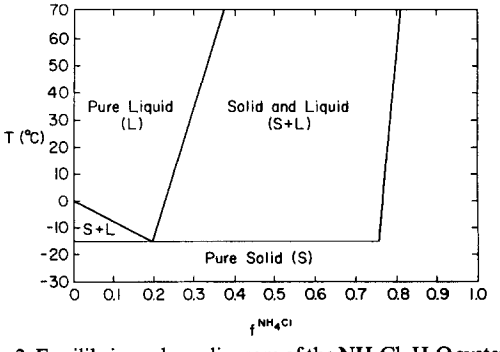

FIG. 2. Equilibrium phase diagram of the NH_4Cl–H_2O system ($T_e = -15.4$°C, $f_e = 0.197$).

peratures changed by more than 1°C over a 15 min period. With an insulated wall at $x = L$, steady state was marked by complete solidification of the solution.

3. EXPERIMENTAL RESULTS

To study the effects of initial solution concentration (f_o) and cold wall temperature (T_c), experiments were performed for the conditions of Table 1. In each case experiments were performed for a heated (H) and an insulated (I) sidewall at $x = L$, yielding a set of ten different operating conditions. By varying the initial mass fraction of NH_4Cl (f_o) from 30 to 10%, results were obtained for solutions located to the right of, at, and to the left of the eutectic point. This variation permitted the study of three fundamentally distinct solidification phenomena. For $f_o = 30\%$ (hypereutectic), solidification is characterized by a two-phase mushy region for which the rejection of water-rich interdendritic fluid results in opposing solutally and thermally driven flows. For a eutectic composition ($f_o = 19.7\%$), solidification exhibits the discrete phase change behavior of a pure substance and flow is driven solely by thermal buoyancy forces. For $f_o = 10\%$ (hypoeutectic), solidification is again characterized by a two-phase mushy region but in this case the rejection of water-lean interdendritic fluid results in mutually augmenting solutal and thermal flows. Experiments involving variations in the cold wall temperature were performed for a single initial concentration ($f_o = 30\%$), for which water-rich interdendritic fluid was rejected from a two-phase region. Hence, the experiments facilitated a study of the effects of changes in the relative magnitudes of the thermal and solutal buoyancy forces on the solidification process.

Solidus and liquidus front development and flow conditions will be discussed for each of the experiments. However, in view of space limitations, presentation of quantitative results will be restricted to case 1 experiments ($f_o = 30\%$) which are of most interest due to the competing nature of the thermal and solutal flows. Due to difficulties associated with photographing double-diffusive interfaces and flow patterns, photographic records will be supplemented with schematic renditions of the flow.

For the eutectic composition, experiments 2-1(H) and 2-1(I), solidification was characterized by a smooth, discrete, solid–liquid interface. The progression of solidification for these cases is shown in Fig. 3. The three thermocouple rakes and the lead wires are clearly seen, as is the fiber-optic refractometer. The effects of thermally driven natural convection were immediately manifested by retardation of solid layer growth near the top of the cavity. Cooling of the fluid at the solid–liquid interface induces a counterclockwise recirculation pattern for which the motion of hot and cold fluid is associated with upper and lower portions of the interface, respectively. The attendant suppression of solidification at the top of the cavity thereby induces non-uniform solid layer growth in the horizontal direction.

Table 1. Experimental conditions

Run	f_o (%)	T_c (°C)
1-1(H or I)	30	−50
1-2(H or I)	30	−30
1-3(H or I)	30	−5
2-1(H or I)	20	−50
3-1(H or I)	10	−50

For the isothermal (heated) wall condition, experiment 2-1(H), steady state is reached at $t \approx 50$ min. At steady state, heat transfer to the bulk liquid from the hot wall is balanced by heat transfer from the liquid to the solid–liquid interface and latent energy is no longer released at the interface. Vertical (y) temperature distributions within the liquid are characterized by stable stratification, while horizontal (x) distributions are characterized by large gradients in boundary layers at the interface and wall and by a nearly isothermal core. As such, conditions are similar to those in a rectangular cavity with differentially heated sidewalls and no change of phase. For the insulated boundary, experiment 2-1(I), the cavity solidifies completely. The initial recirculation in the melt is strong, as for the heated wall, but weakens considerably as the temperature of the insulated wall decreases. Therefore, solid layer growth at the top of the cavity is suppressed up to $t \approx 20$ min, after which the insulated wall has cooled significantly, recirculation is greatly diminished, and there is nearly uniform growth along the entire solid–liquid interface.

Solutal buoyancy forces become important for mixtures of non-eutectic composition. As the mushy region is formed for the hypoeutectic conditions of experiments 3-1(H) and 3-1(I), its liquid phase NH_4Cl concentration and temperature increase and decrease, respectively, relative to conditions in the adjoining pure liquid or melt. Hence, the mushy zone liquid is denser than the melt, creating conditions conducive to a solutally and thermally driven downflow along the liquidus interface and counterclockwise recirculation in the melt. Due to cooling of the bulk fluid as it descends along the liquidus and the expulsion of liquid from the mushy zone, cool, solute-rich conditions develop at the bottom of the cavity. Despite the near eutectic composition of the solution, its lower temperature enhances advancement of both the solidus and liquidus fronts at the test cell bottom (Fig. 4). In contrast, as in eutectic solidification, growth is retarded at the top of the cavity due to thermally driven natural convection. Relative to the eutectic composition, solidification is initially enhanced by the outflow of cold fluid from the mushy zone and by the existence of an initial liquidus temperature which is 8°C larger than the eutectic temperature. Outflow of solute-rich fluid from the mushy region creates a solut-

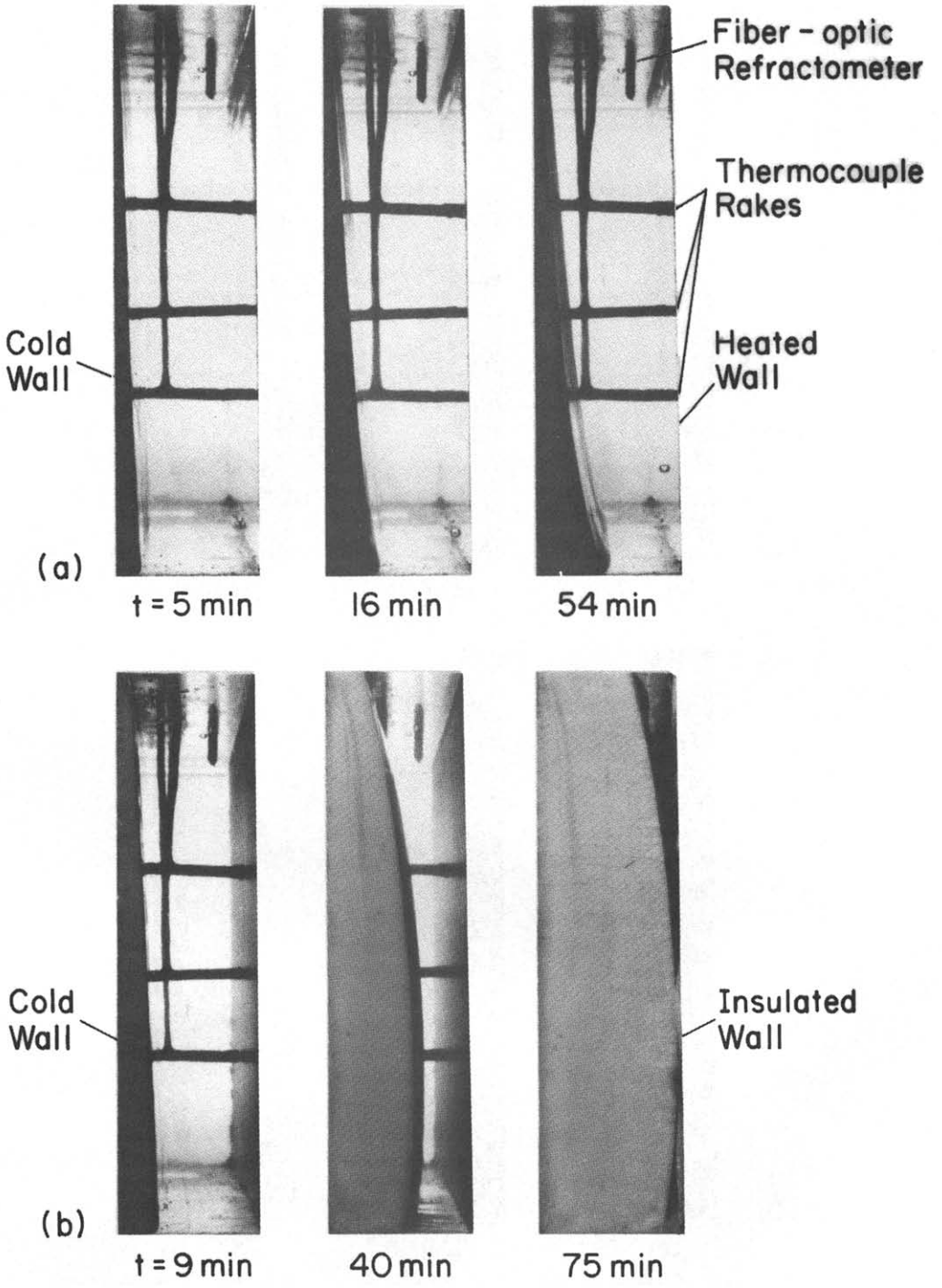

FIG. 3. Solidification morphology at selected times for (a) experiment 2-1(H) and (b) experiment 2-1(I).

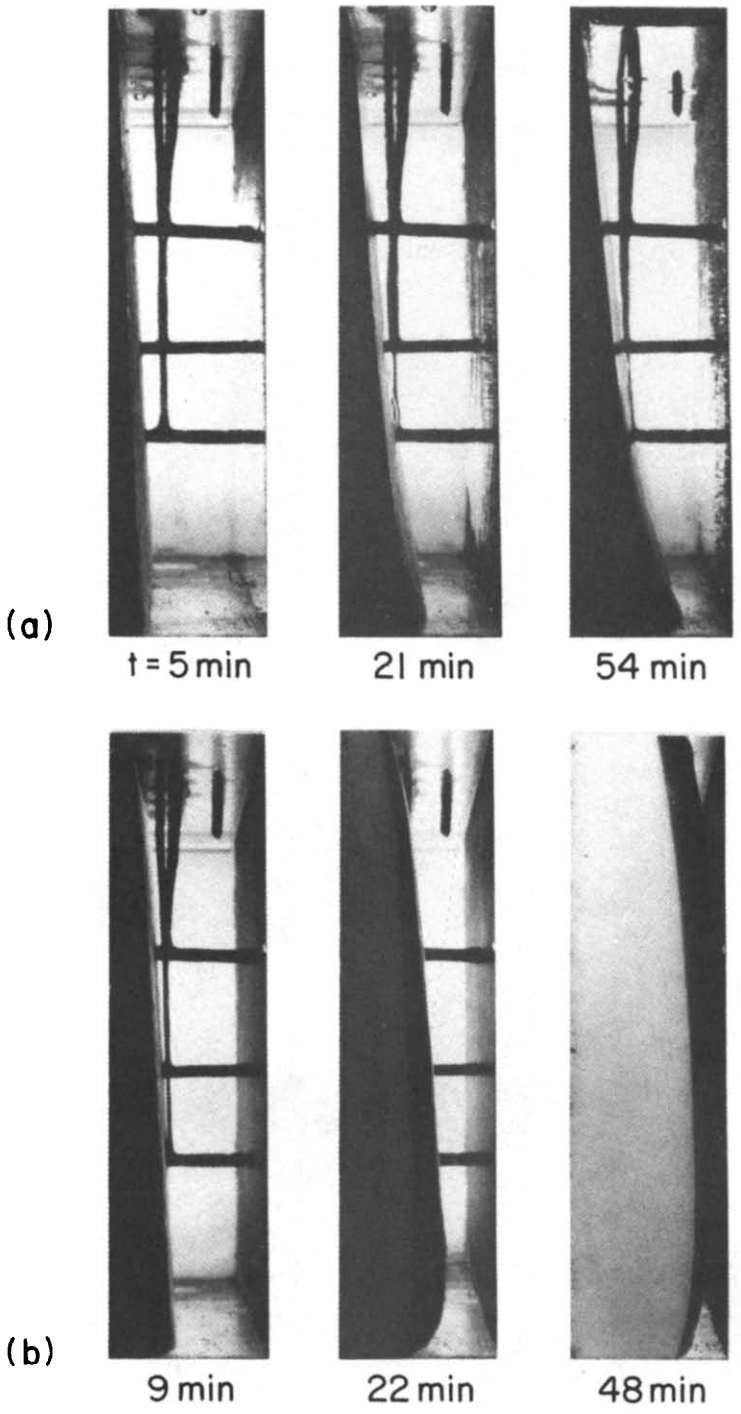

FIG. 4. Solidification morphology at selected times for (a) experiment 3-1(H) and (b) experiment 3-1(I).

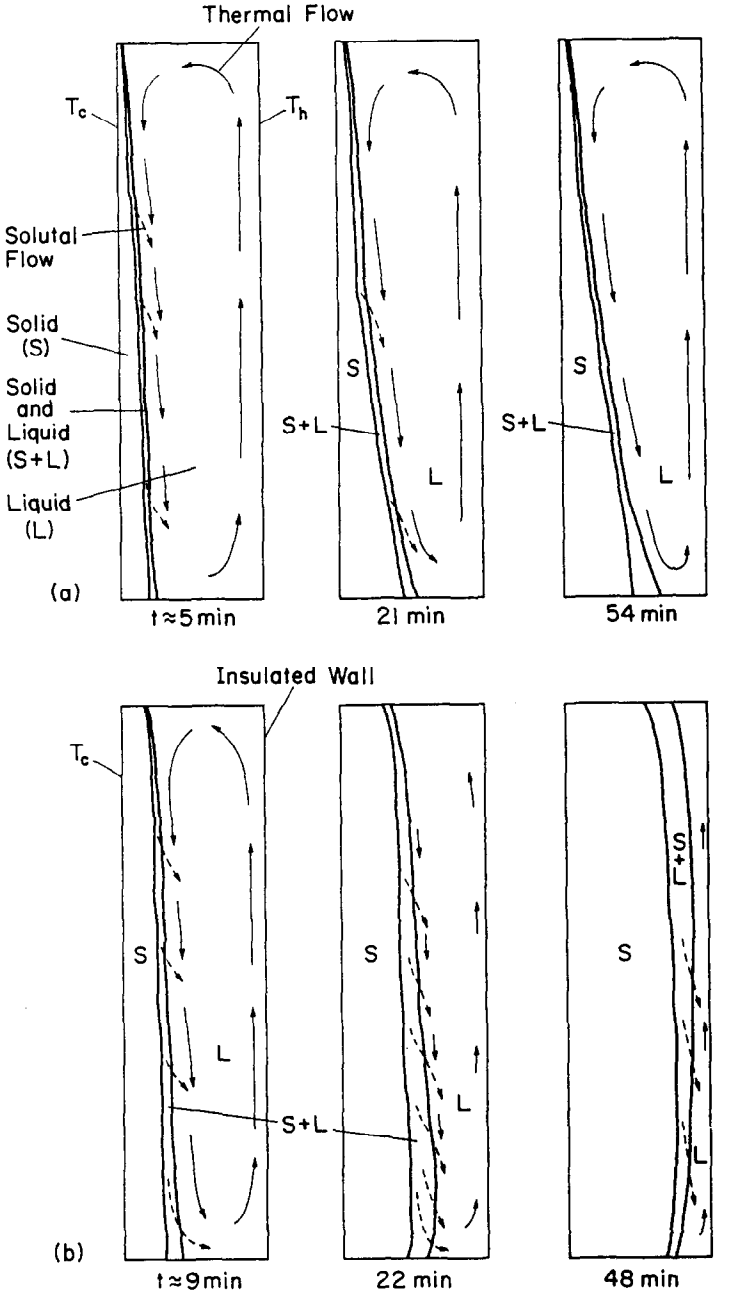

FIG. 5. Solidification morphology and flow patterns at selected times for (a) experiment 3-1(H) and (b) experiment 3-1(I).

ally driven downflow at the liquidus which enhances the thermally driven flow (Fig. 5).

In experiment 3-1(H), steady state is reached after approximately 1 h. Throughout experiment 3-1(H) and in the early stages of 3-1(I), conditions are similar to those of thermally driven natural convection in a cavity. That is, conditions are thermally stratified with descending and ascending boundary layer flows at the cooled and heated boundaries, respectively. As shown in Fig. 5, the thermally driven downflow along the liquidus (solid arrows) is augmented by the solutal flow (dashed arrows). It is this downflow of solute-rich fluid which causes a weak reversal in liquidus front development at the bottom of the cavity. The effect is most pronounced at intermediate times for experiment 3-1(I), as shown in Figs. 4(b) and 5(b). Hence, in experiment 3-1(I), the front, which is initially more advanced at the bottom than at the top due to thermally induced recirculation, gradually thickens at the top and thins at the bottom. Due to a diminishing influence of the thermally driven flow, as shown by the decreasing size of the solid arrows in Fig. 5(b), descending solute-rich fluid tends to remain at the cavity bottom, thereby inhibiting the growth of mush by reducing the liquidus temperature. In contrast, growth of mush at the top is enhanced by the reduction in melt temperature and the strength of the thermally driven recirculation. Accordingly, the top and bottom portions of the cavity are the last to solidify, with complete solidification occurring at approximately 70 min. Solid and mushy region thicknesses depicted in Fig. 5 were determined from the photographs of Fig. 4. The association of sharp changes in contrast in the photographs with the solidus and liquidus interfaces was confirmed by temperature data and by physical probing of the solidified material. Although conditions are conducive to the double-diffusive layering observed by Thompson and Szekely [19], particularly for the heated wall, such layers were not observed in this study.

Conditions are most interesting when solidification occurs to the right of the eutectic point and solutal and thermal buoyancy forces are opposing. Unlike behavior for experiments 2-1 and 3-1, results for experiment 1-1(H) reveal an irregular liquidus interface which is characteristic of dendritic growth. As shown schematically in Fig. 6(a), solidus and liquidus growth are initially planar, with the solid and mushy regions having approximately the same thickness. Again these thicknesses are determined from the associated photographic records. However, as the solid forms, cooler, solute-deficient fluid is ejected from the mushy region and rises to the top of the cavity. Although a strong thermally induced, counterclockwise circulation still exists in the liquid, it is now opposed by the ascending solutally driven flow and vigorous mixing is induced at the liquidus interface. Conditions become double-diffusive in the sense that thermally unstable (cooler over warmer) but solutally stable (solute-deficient over solute-rich) fluid accumulates at the top of the cavity to form a thin convecting layer which is separated from the remaining bulk liquid by an interface (Fig. 6(b)). The top layer is characterized by a nearly uniform concentration and temperature and experiences a counterclockwise, thermally-induced circulation.

An accumulation of cold, solute-deficient fluid above the double-diffusive interface inhibits further

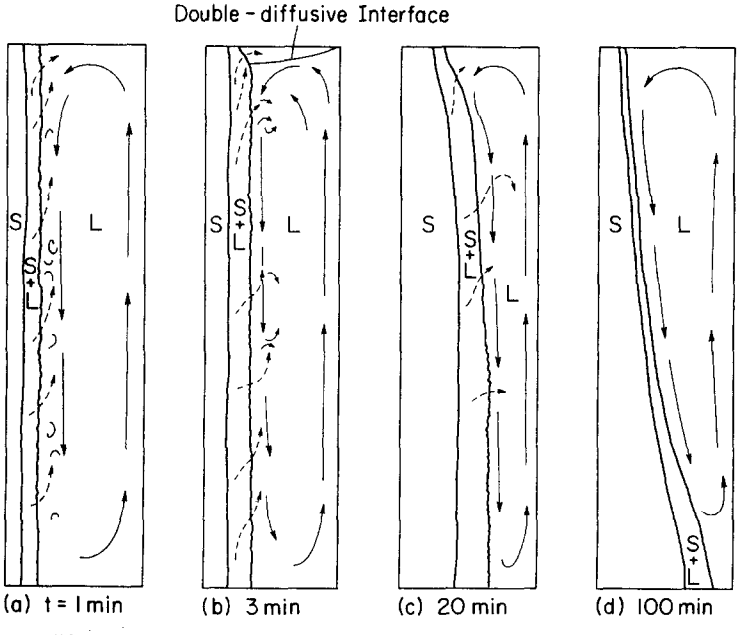

FIG. 6. Solidification morphology and flow patterns at selected times for experiment 1-1(H).

development of the liquidus. In fact, because the decreasing NH_4Cl concentration of the adjoining liquid corresponds to a decrease in liquidus temperature, there is local remelting. Remelting also results from the impingement of warm fluid from the heated wall on the liquidus interface. However, due to the large liquidus slope (Fig. 2), small changes in concentration induce large changes in liquidus temperature and remelting is strongly influenced by solutal effects.

In this experiment, the double-diffusive interface does not persist for long, as species and thermal energy transfer across the interface act to equilibrate the adjoining convection layers and produce a single well-mixed melt. Normal and shear forces imparted by strong thermal convection in the bulk fluid also contribute to erosion of the double-diffusive interface. The interface is destroyed shortly after it is formed and a single well-mixed region exists for $t \geqslant 5$ min. Subsequent solutally driven outflow from the mushy region is swept into the melt by the thermally driven flow (Fig. 6(c)). A steady-state condition is reached at $t \approx 100$ min, and the buoyancy driven flow is limited to thermal convection in the melt. The dendritic surface is eroded by this flow, and a smooth liquidus surface is attained (Fig. 6(d)).

In experiment 1-1(I), an initially strong, thermally induced, counterclockwise circulation weakens as the insulated wall cools. Accordingly, conditions favor the formation of double-diffusive interfaces, and three such interfaces were observed to form as solute-deficient interdendritic fluid streamed into the melt (Figs. 7(a) and (b)). The layers grew in the downward direction as solidification progressed, with each layer exhibiting a weak counterclockwise, thermally induced circulation. Small temperature differences between the adjoining convection layers limited heat transfer and the layers remained independent through most of the solidification process. The solidification rate slowed considerably near the end of the process, as a stagnant pool of nearly eutectic liquid accumulated near the insulated wall at the top of the cavity (Fig. 7(c)). Complete solidification occurred after approximately 2 h. Multiple double-diffusive interfaces have also been observed when horizontal temperature and concentration gradients are imposed on a large aspect ratio enclosure with no solidification [26].

To examine the importance of thermal effects on the solidification process, the initial liquid composition was held constant at $f_o = 30\%$ while the cold wall temperature was varied. Experiments 1-2(H) and 1-2(I) were performed with a cold wall temperature of $T_c = -30°C$, and the progression of solidification is shown in Fig. 8. In such observations, the solidus interface provided a boundary between lighter (solid) and darker (mushy) zones, and thin white (Fig. 8(a)) or black (Fig. 8(b)) lines have been added to highlight the solidus. Since it reflects less of the incident light, the mushy region appears darker than the solid. This interpretation was confirmed by physical probing of the solidified material.

At early and intermediate times, the rejection of interdendritic fluid into the melt for experiment 1-2(H) is revealed by striations (irregular variations in contrast) in the bulk fluid near the liquidus (Fig. 8(a)). Striations due to liquid density gradients also reveal a double-diffusive interface near the top of the cavity

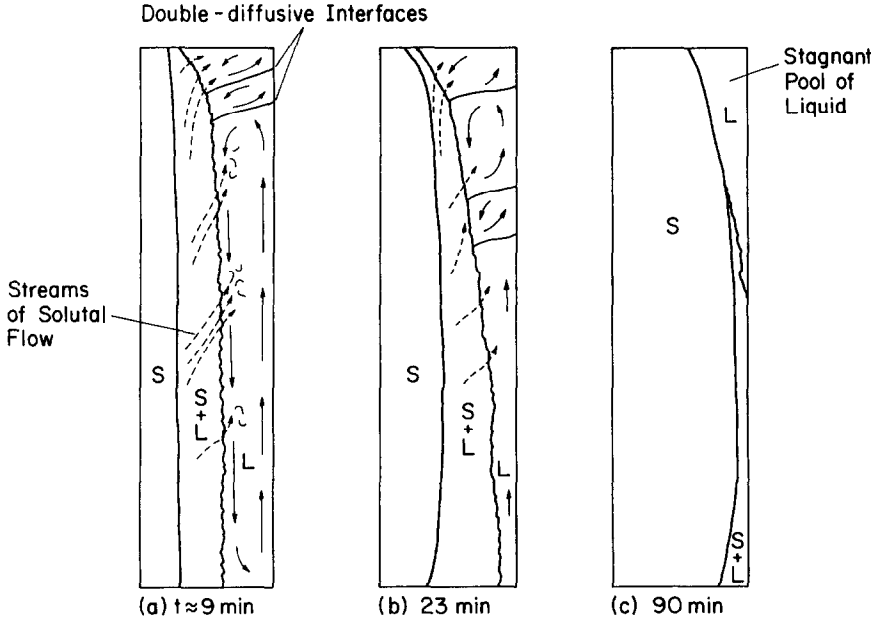

FIG. 7. Solidification morphology and flow patterns at selected times for experiment 1-1(I).

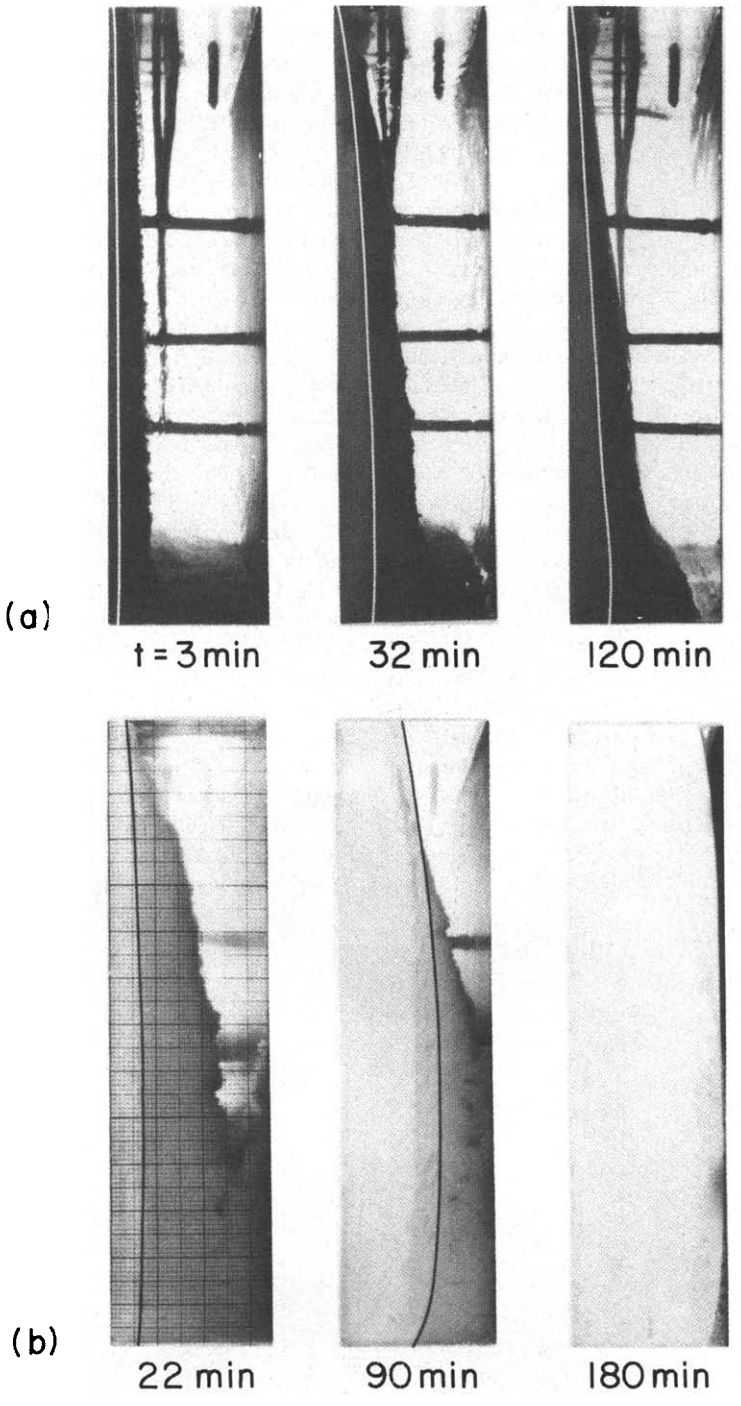

FIG. 8. Solidification morphology at selected times for (a) experiment 1-2(H) and (b) experiment 1-2(I).

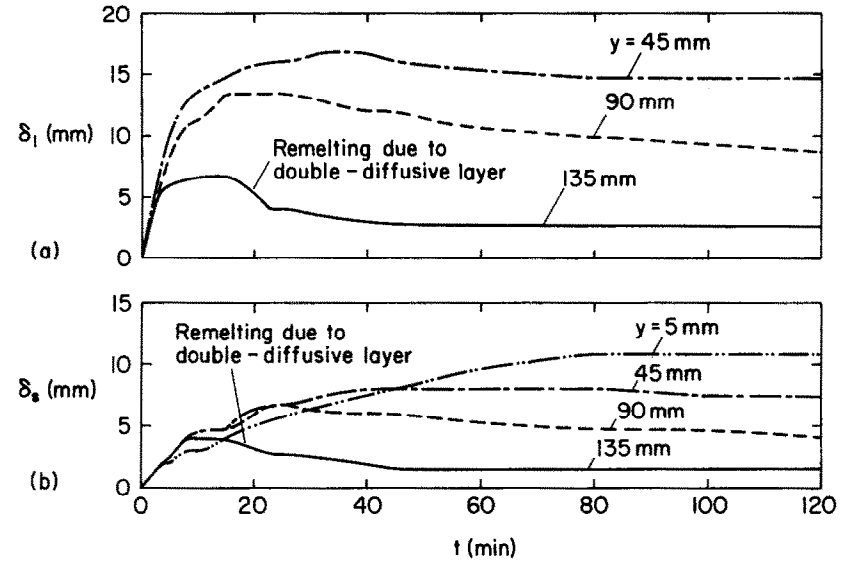

FIG. 9. Liquidus (a) and solidus (b) thicknesses as a function of time for selected vertical locations in the cavity: experiment 1-2(H).

and an ascending thermal boundary layer along the heated wall. Liquidus and solidus interface locations determined from photographs such as those of Fig. 8(a) are shown in Fig. 9. The uncertainty in locating interface positions from the photographs is ± 0.25 mm, and the corresponding solidus locations are within ± 0.5 mm of results inferred from temperature measurements. Figure 10 presents the output of the fiber-optic refractometer, and temperature histories are shown in Fig. 11. The temperature histories are numbered in sequence from the cold wall according to their respective x locations (Fig. 1). Data absent from the figure correspond to locations at which thermocouples were lost due to corrosion.

Solidification for experiment 1-2(H) is similar to that for experiment 1-1(H), although thermal effects are less pronounced due to the smaller temperature difference across the cavity sidewalls. Since fluid discharged from the mush is not as cold, there is less heat transfer across the double-diffusive interface which forms early in the process. Moreover, the thermally driven flow in the melt below the interface is weaker, and breakdown of the interface is delayed. Hence, the top layer grows to a greater extent (Fig. 12(b)) until the interface eventually disintegrates and formation of a well-mixed melt characterized by counterclockwise thermal circulation leads to steady-state conditions.

Initially, the mushy region grows much faster than

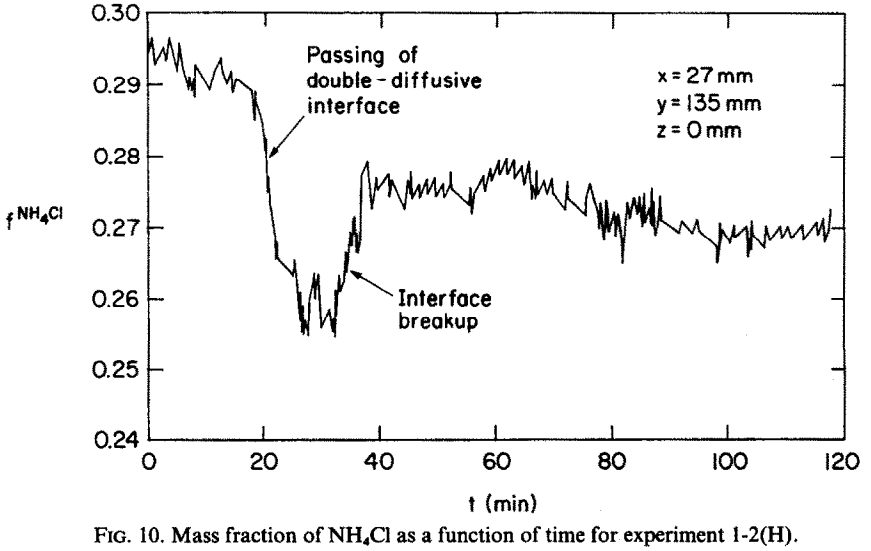

FIG. 10. Mass fraction of NH_4Cl as a function of time for experiment 1-2(H).

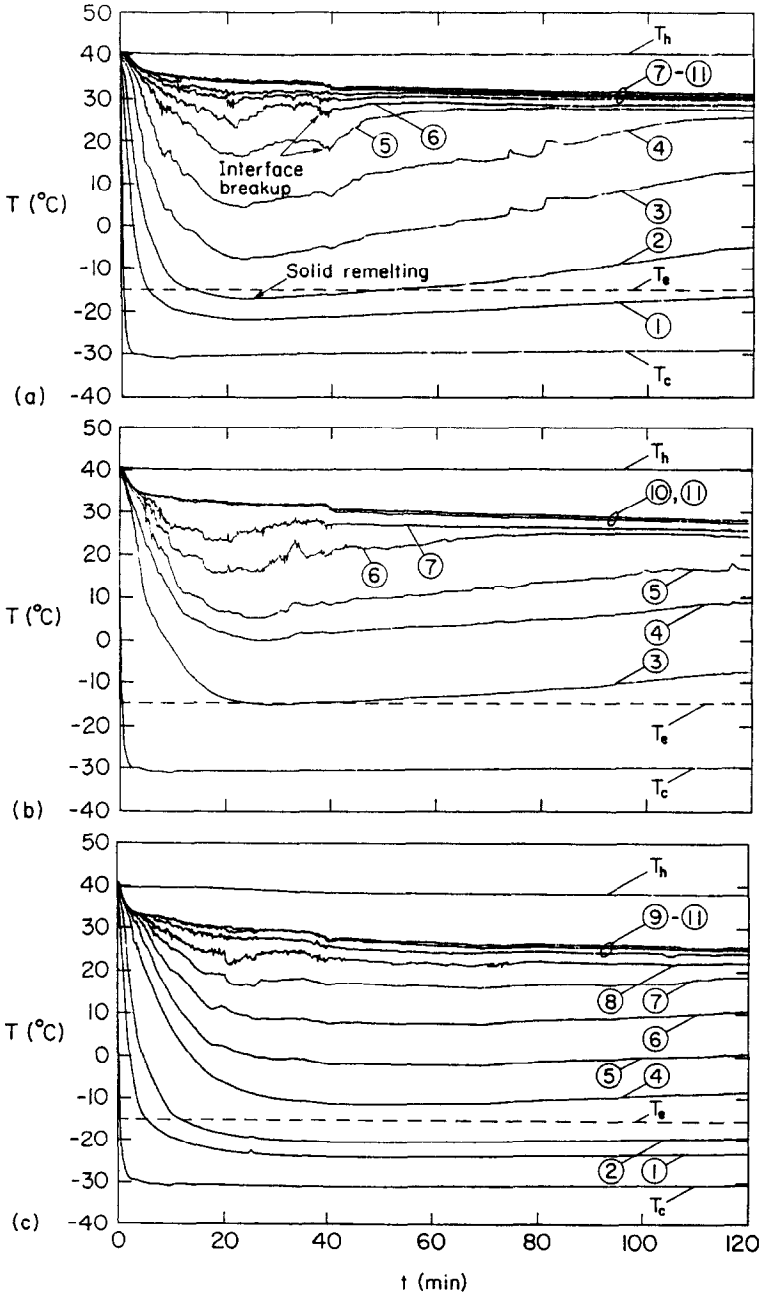

FIG. 11. Temperature histories at different x locations for experiment 1-2(H): (a) $y = 90$ mm; (b) $y = 65$ mm; (c) $y = 45$ mm.

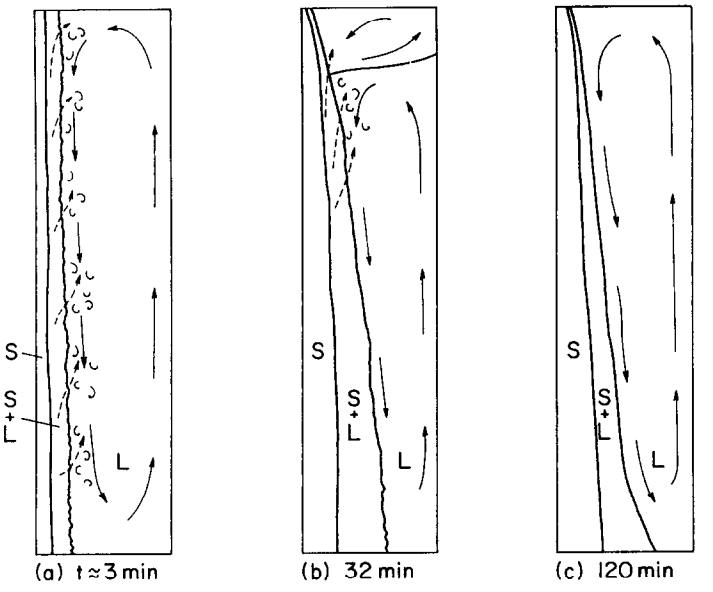

FIG. 12. Solidification morphology and flow patterns at selected times for experiment 1-2(H).

the solid, as indicated by the differences in slopes of the solidus and liquidus interface curves (Fig. 9). Moreover, up to $t \approx 25$ min, gradual cooling occurs throughout the cavity. However, beyond this time warming of both bulk and interdendritic fluids occurs. For example, temperature histories 3 (interdendritic fluid) and 5 (bulk fluid) of Fig. 11(a) both increase after $t \approx 25$ min. This result indicates that, not only is the bulk fluid being heated by the hot wall, but the interdendritic fluid is also being heated through interaction of the bulk and mushy region flows. As a result, the entire liquidus front undergoes slight remelting (Fig. 9(a)), as the effect of the heated wall propagates to the mushy region. Remelting of the mush begins at the top ($y = 135$ mm) at $t \approx 15$ min and progresses downward, subsequently occurring at $t \approx 20$ min for $y = 90$ mm and at $t \approx 40$ min for $y = 45$ mm.

Due to the solutal flows originating in the mushy region, a single double-diffusive interface forms and descends from the top of the cavity (Fig. 12(b)). As shown in Fig. 10, the concentration in this region remains approximately constant until $t \approx 20$ min, when a sudden 3.5% decrease occurs. This decrease corresponds to downward movement of the double-diffusive interface past the probe tip, and as shown in Fig. 8(a) at $t = 32$ min and Fig. 12(b), there is extensive remelting of the mushy region adjoining the double-diffusive layer. However, at $t \approx 40$ min, the concentration at the top of the cavity suddenly increases by 1.5%, indicating breakup of the double-diffusive interface and associated mixing of solute-rich fluid from the bottom region with solute-deficient fluid in the top layer. As shown in Fig. 11(a), breakup of the interface at $t \approx 40$ min also decreases temperatures below the interface due to mixing of the cooler top layer fluid with warmer fluid in the bottom region. A single well-mixed region results, and steady state follows at $t \approx 120$ min. Once again, the cessation of solidification and thermal circulation in the melt yield a smooth liquidus for the steady-state condition (Fig. 8(a)). Because of the larger cold wall temperature, the extent of the solidification, as measured by the mass of solid formed, is nearly half that of experiment 1-1(H).

A photographic account of solidification for experiment 1-2(I) is shown in Fig. 8(b), and corresponding liquidus and solidus interface locations are plotted in Fig. 13. Concentration and temperature histories within the cavity are presented in Figs. 14 and 15, respectively. For $t = 22$ min in Fig. 8(b), the photograph was taken with a superimposed transparent grid. Although similar to results for experiment 1-1(I), the solidification process required a much longer time (~ 180 min) to reach steady state. Once again, an initially strong thermally induced circulation gradually subsided, while double-diffusive phenomena became prominent.

Interface positions (Fig. 13) indicate that, initially, the mushy layer grows much faster than the solid, and at $t = 9$ min it is approximately twice as thick. Large quantities of solute-deficient fluid ascend from the mushy region and two double-diffusive interfaces, which form early in the solidification process, descend rapidly with increasing time (Figs. 16(a) and (b)). Downward propagation of the upper interface is evident from the concentration data of Fig. 14, which reveals a large decrease at $t \approx 10$ min. Downward propagation of both interfaces is evident from the temperature data of Fig. 15(a), which reveal at least

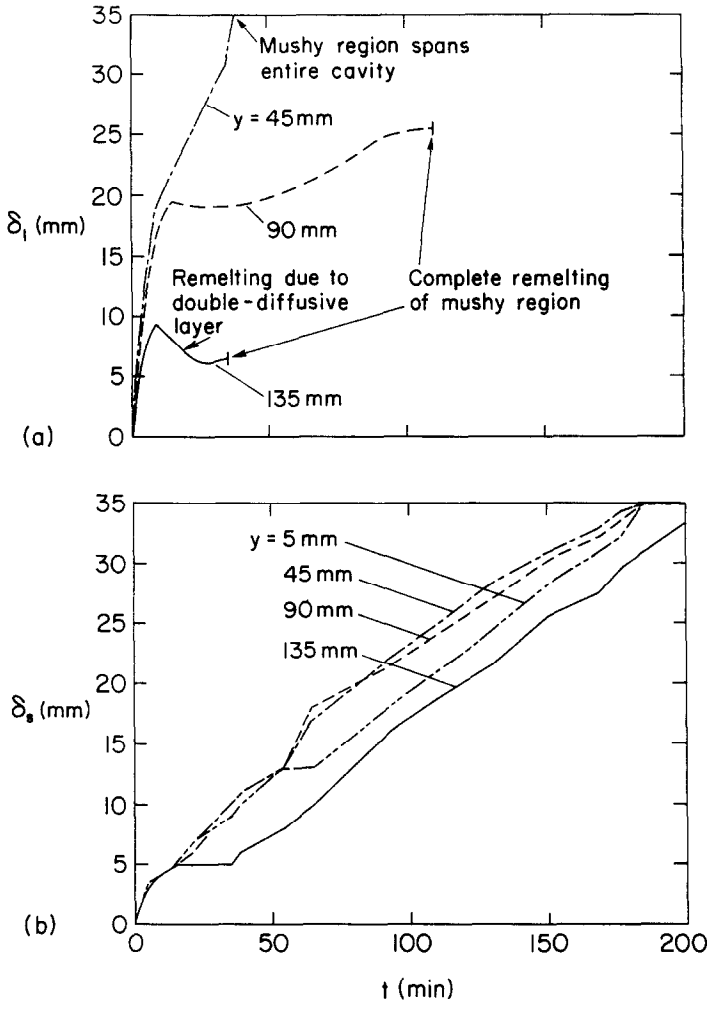

FIG. 13. Liquidus (a) and solidus (b) thicknesses as a function of time for selected vertical locations in the cavity: experiment 1-2(I).

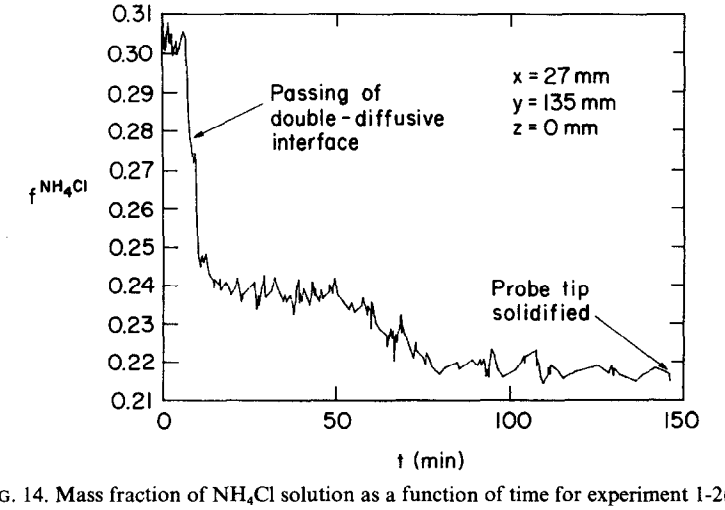

FIG. 14. Mass fraction of NH_4Cl solution as a function of time for experiment 1-2(I).

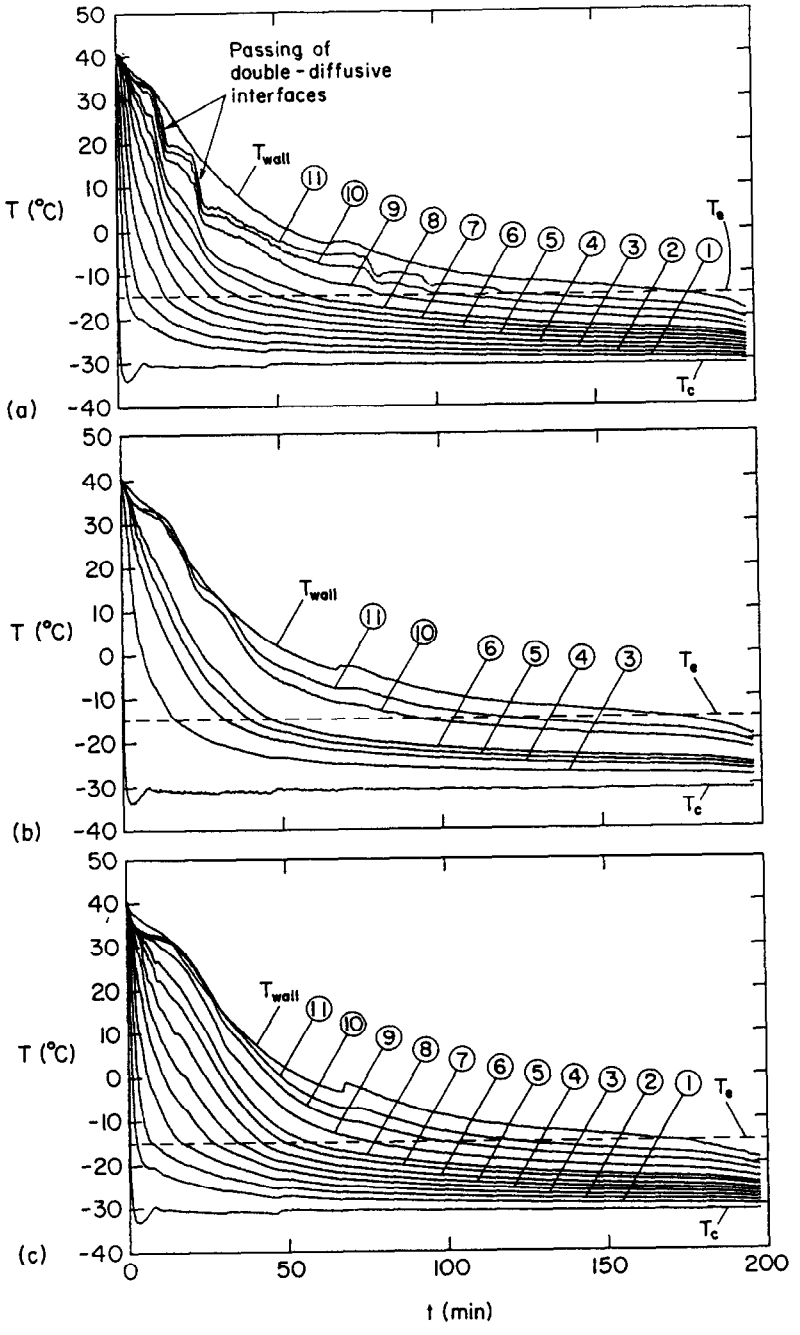

FIG. 15. Temperature histories at different x locations for experiment 1-2(I): (a) $y = 90$ mm; (b) $y = 65$ mm; (c) $y = 45$ mm.

two large drops from $t = 0$ to 50 min. Remelting is extensive, and within 110 min the mushy region is completely eliminated in the upper half of the cavity (Fig. 13(a)) due to the accumulation of solute-deficient fluid in that region. In contrast, solutal conditions at the bottom of the cavity remain nearly unchanged throughout the solidification process, and a two-phase, mushy zone persists until complete solidification of the cavity occurs at $t \approx 180$ min. Overall, the concentration in the melt changes by 8% (Fig. 14). As shown in Fig. 15(a), interaction of the interdendritic and bulk fluid flows is revealed by sharp temperature reductions within the mushy region (temperature histories 7 and 8) at times corresponding to passage of double-diffusive interfaces in the melt (temperature histories 9–11).

The effects of a further increase in cold wall temperature to $T_c = -5°C$, experiment 1-3(H), are shown in Figs. 17(a)–21. Since the cold wall temperature exceeds the eutectic temperature, a pure solid does not form. Counterclockwise circulation due to thermal effects and the formation of a single double-diffusive interface occur, as in the previous cases. However, due to the larger cold wall temperature, the interface remains longer and penetrates further down the cavity. The interface is prominent in Fig. 17(a) at $t = 79$ min, and its development is shown in Fig. 21. In this case, there is nearly complete remelting of the mushy region adjoining the convection layer above the interface. At $t \approx 100$ min, complete breakup of the double-diffusive interface induces significant concentration and temperature changes at the measurement locations (Figs. 19 and 20). Subsequently, there is a gradual smoothing of the liquidus interface due to the thermally driven flow. Steady state is reached at $t \approx 120$ min.

For experiment 1-3(I), Figs. 17(b) and 22, double-diffusive effects and remelting were again present. Temperature and concentration histories, as well as visual observations, revealed three double-diffusive interfaces which descended in the melt with increasing time (Fig. 22). Complete remelting of the mush near the top of the cavity occurred early due to solutal effects. Fluid motion was indiscernible at $t \approx 60$ min and further solidification was negligible, since the cold wall temperature was not sufficiently low to solidify fluid of nearly eutectic composition. Erosion of dendritic arms at the liquidus interface did not occur, and the double-diffusive interfaces did not decompose prior to completion of the experiment.

4. SUMMARY

An experimental study of solidification for a binary mixture in a rectangular cavity has been conducted using aqueous ammonium chloride as the phase change material. By varying the initial NH_4Cl concentration, the cold wall temperature, and the thermal condition of the opposing wall, experiments were performed to examine the effects of thermally and solutally driven flows on the solidification process.

Initial concentrations which are less than the eutec-

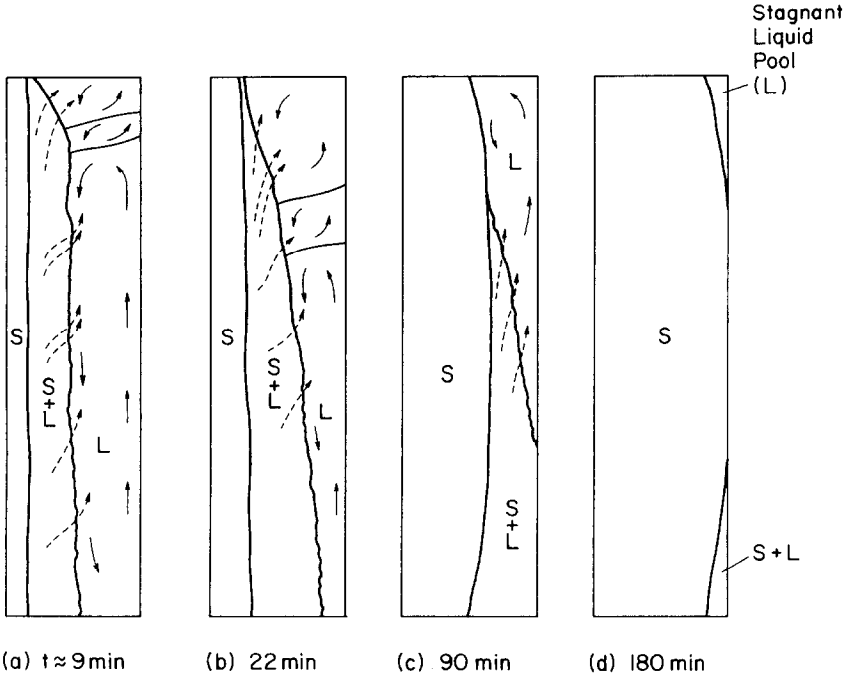

FIG. 16. Solidification morphology and flow patterns at selected times for experiment 1-2(I).

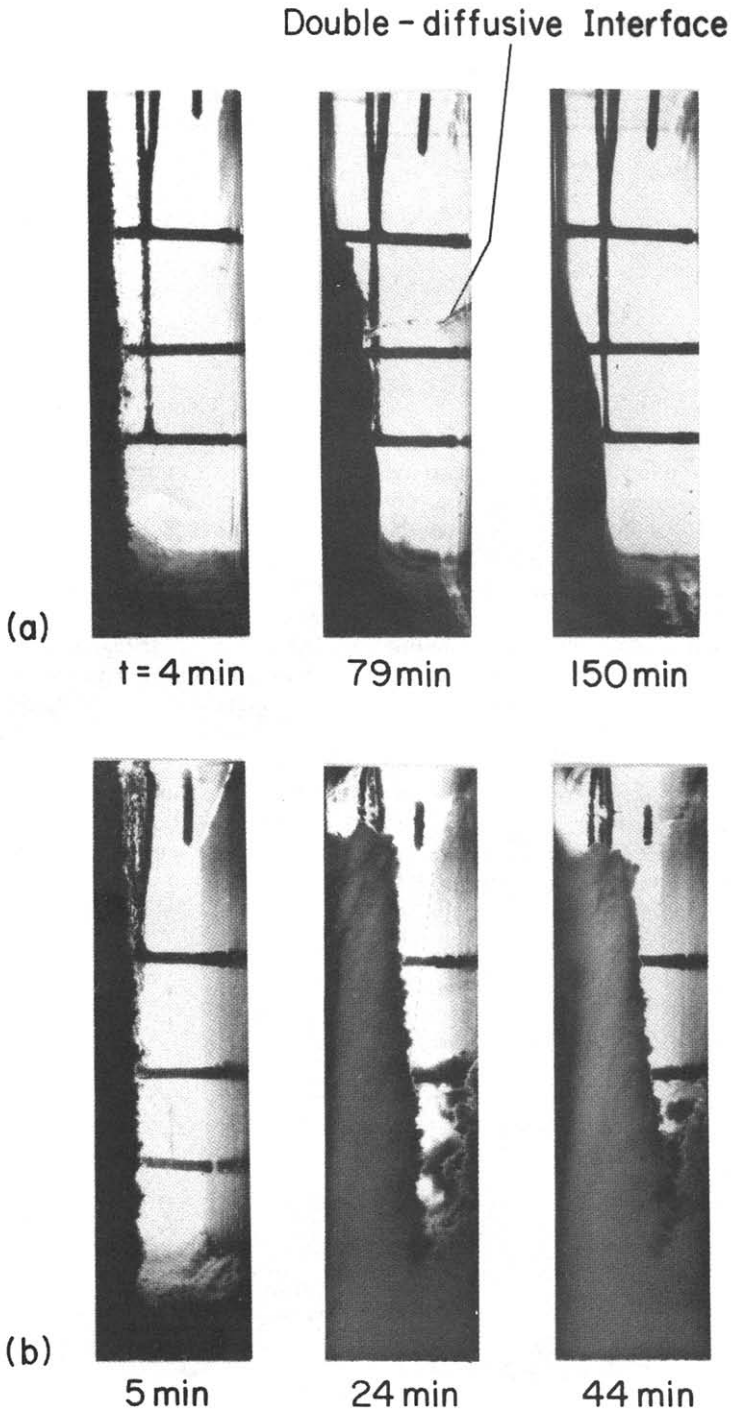

FIG. 17. Solidification morphology at selected times for (a) experiment 1-3(H) and (b) experiment 1-3(I).

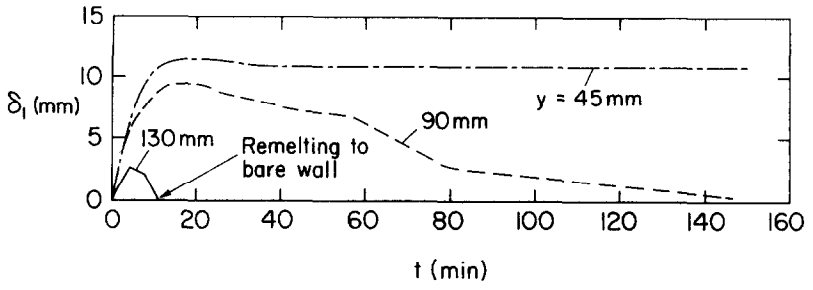

FIG. 18. Liquidus thickness as a function of time for selected vertical locations in the cavity: experiment 1-3(H).

tic concentration produce solutal flows that aid thermally driven downflow along the liquidus interface, while concentrations greater than the eutectic produce an ascending solutal flow which opposes the thermal flow. In the opposing case, solute (NH_4Cl) deficient fluid is ejected from the mushy region and rises to create double-diffusive conditions at the top of the cavity. In both cases, solute redistribution occurs as a result of the solutal flow, and localized liquid regions of near eutectic composition retard growth and cause remelting of solid in the mushy region.

The relative strengths of ascending solutal and counterrotating thermal flows determine the extent of double-diffusive effects and solute redistribution. By decreasing the temperature difference across the cavity (increasing the cold wall temperature), solutal flows exert an increasingly more important effect on the solidification process. Solidification rates decrease and localized remelting due to double-diffusive layering increases as thermal effects are reduced. Similarly, the effect of the solutal flow becomes more pronounced when the opposite sidewall is insulated, instead of being maintained at the initial temperature of the solution.

The structure of the liquidus front also depends on thermal and solutal conditions. Initial concentrations less than or equal to the eutectic produce a smooth liquidus interface, while concentrations greater than the eutectic result in a jagged, irregular liquidus front. If thermal effects are dominant, as, for example, when the opposing wall is heated and the cold wall is maintained at a low temperature, erosion at the liquidus interface results in smoothing of the initially irregular surface.

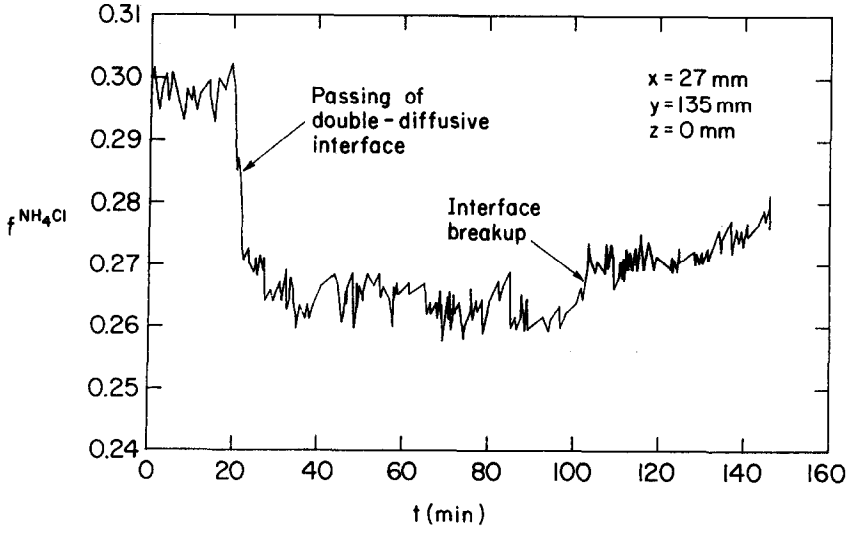

FIG. 19. Mass fraction of NH_4Cl solution as a function of time for experiment 1-3(H).

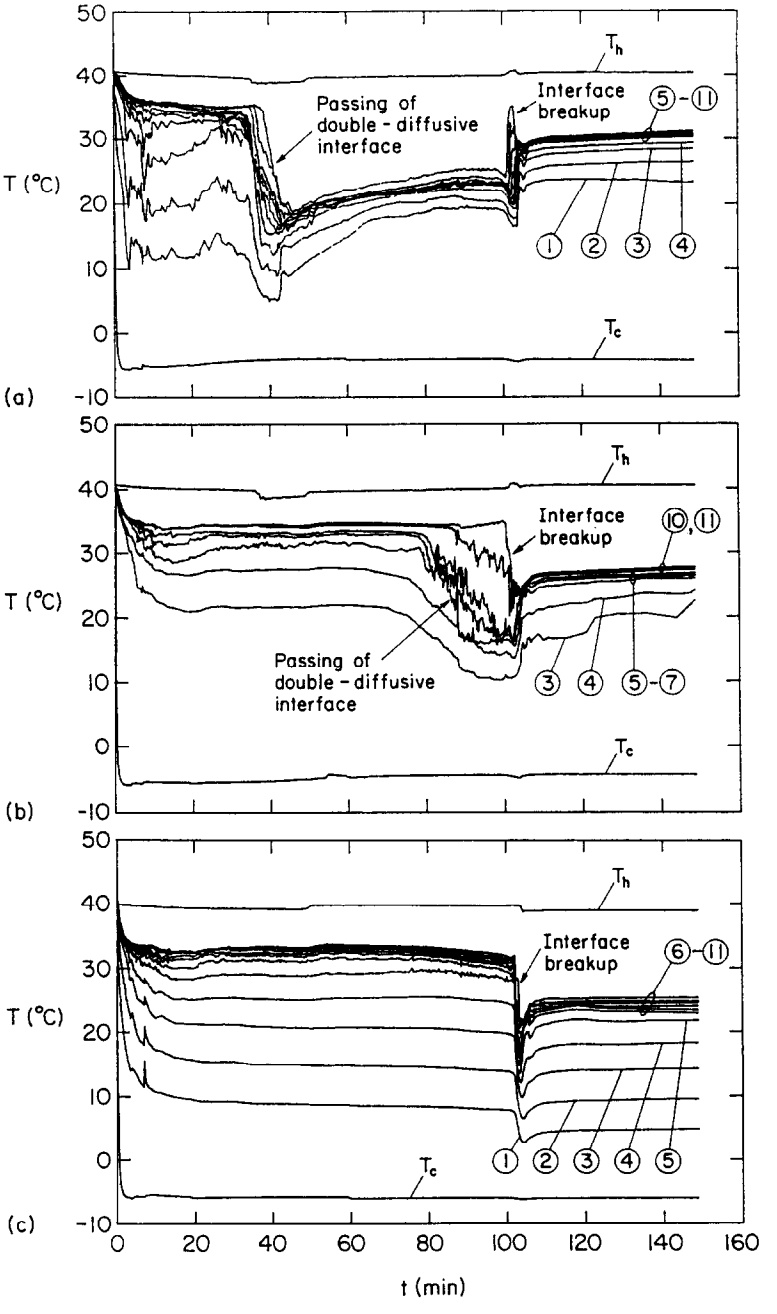

FIG. 20. Temperature histories at different x locations for experiment 1-3(H): (a) $y = 90$ mm; (b) $y = 65$ mm; (c) $y = 45$ mm.

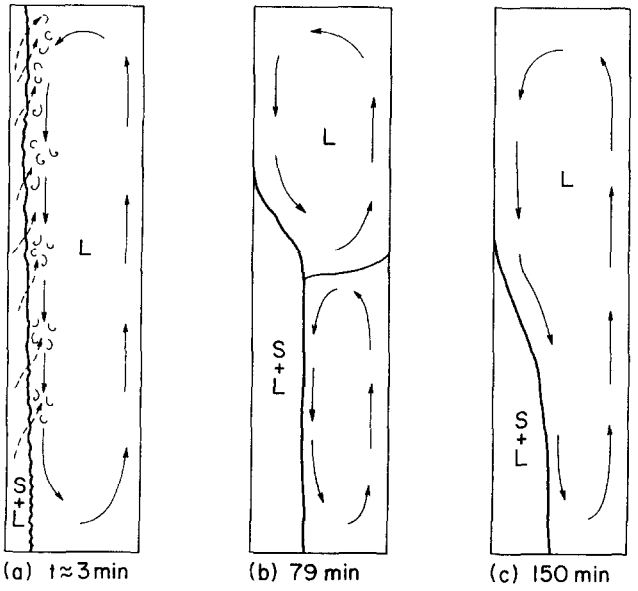

FIG. 21. Solidification morphology and flow patterns at selected times for experiment 1-3(H).

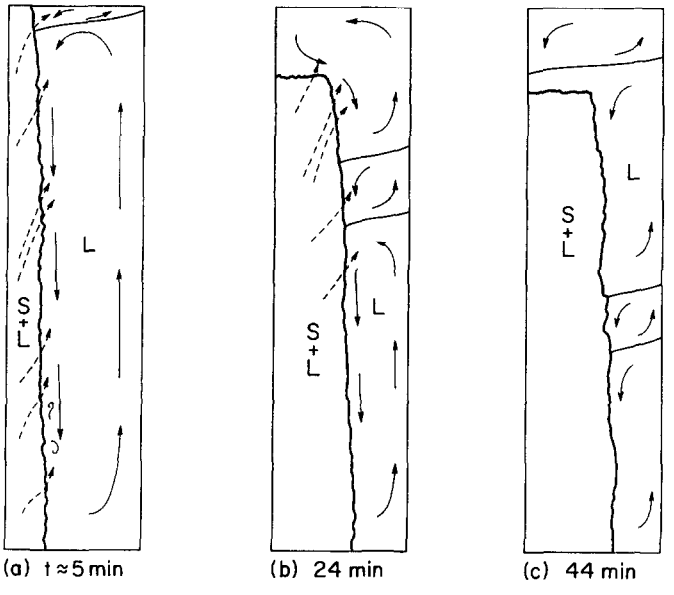

FIG. 22. Solidification morphology and flow patterns at selected times for experiment 1-3(I).

Acknowledgement—Support of this work by the U.S. Department of Energy (Office of Basic Energy Sciences) under Grant No. DE-FG02-87ER13759 is gratefully acknowledged.

REFERENCES

1. S. Ostrach, Fluid mechanics in crystal growth—The 1982 Freeman Scholar Lecture, *J. Fluids Engr* **105,** 5–20 (1983).
2. G. A. Lane, *Solar Heat Storage: Latent Heat Material*, Vol. I. CRC Press, Boca Raton, Florida (1983).
3. K. M. Fisher, The effects of fluid flow on the solidification of industrial castings and ingots, *Physico-Chem. Hydrodyn.* **2,** 311–326 (1981).
4. G. M. Oreper and J. Szekely, Heat and fluid flow phenomena in weld pools, *J. Fluid Mech.* **147,** 53–79 (1984).
5. H. E. Huppert and R. S. J. Sparks, Double-diffusive convection due to crystallization in magmas, *Ann. Rev. Earth Planet. Sci.* **12,** 11–37 (1984).
6. H. E. Huppert and J. S. Turner, Ice blocks melting into a salinity gradient, *J. Fluid Mech.* **100,** 367–384 (1980).
7. R. Viskanta, Natural convection in melting and solidification. In *Natural Convection* (Edited by S. Kakac, W. Aung and R. Viskanta), pp. 845–877. Hemisphere, New York (1985).
8. R. Viskanta, Phase change heat transfer. In *Solar Heat Storage: Latent Heat Material* (Edited by G. A. Lane), Vol. I, pp. 153–222. CRC Press, Boca Raton, Florida (1983).
9. M. C. Flemings, Principles of control of soundness and homogeneity of large ingots, *Scand. J. Metallurgy* **5,** 1–15 (1976).
10. R. Mehrabian, M. A. Keane and M. C. Flemings, Experiments on macrosegregation and freckle formation, *Met. Trans.* **1,** 3238–3241 (1970).
11. R. J. McDonald and J. D. Hunt, Fluid motion through the partially solid regions of a casting and its importance in understanding A type segregation, *Trans. Metall. Soc. A.I.M.E.* **245,** 1993–1997 (1969).
12. S. Asai and I. Muchi, Theoretical analysis and model experiments on the formation mechanism of channel-type segregation, *Trans. ISIJ* **18,** 90–98 (1978).
13. M. J. Stewart and F. Weinberg, Fluid flow through a solid–liquid dendritic interface, *Met. Trans.* **3,** 333–337 (1972).
14. A. Sample and A. Hellawell, The effect of mold precession on channel and macro-segregation in ammonium chloride–water analog castings, *Met. Trans. B* **13B,** 495–501 (1982).
15. S. Witzke, J.-P. Riquet and F. Durand, Visualisation de la convection lors de la cristallisation basaltique et equiaxe d'une solution transparente, *Mem. Scient. Revue Metall.* **76,** 701–714 (1979).
16. K. Murakami and T. Okamoto, Formation of equiaxed zone in castings, *Metal Sci.* **18,** 103–111 (1984).
17. J. Szekely and A. S. Jassal, An experimental and analytical study of the solidification of a binary dendritic system, *Met. Trans. B* **9B,** 389–398 (1978).
18. J. S. Turner, Multicomponent convection, *Ann. Rev. Fluid Mech.* **17,** 11–44 (1985).
19. M. E. Thompson and J. Szekely, Mathematical and physical modeling of double-diffusive convection of aqueous solutions crystallizing at a vertical wall, *J. Fluid Mech.* **187,** 409–433 (1988).
20. C. F. Chen, Onset of cellular convection in a salinity gradient due to a lateral temperature gradient, *J. Fluid Mech.* **63,** 563–576 (1974).
21. C. Beckermann, Melting and solidification of binary mixtures with double-diffusive convection in the melt, Ph.D. Thesis, Purdue University (1987).
22. M. S. Christenson, W. D. Bennon and F. P. Incropera, Solidification of an aqueous ammonium chloride solution in a rectangular cavity—II. Comparison of predicted and measured results, *Int. J. Heat Mass Transfer* **32,** 69–79 (1989).
23. W. D. Bennon and F. P. Incropera, A continuum model for momentum, heat and species transport in binary solid–liquid phase change systems—I. Model formulation, *Int. J. Heat Mass Transfer* **30,** 2161–2170 (1987).
24. T. L. Bergman, F. P. Incropera and W. H. Stevenson, Miniature fiber-optic refractometer for measurement of salinity in double-diffusive thermohaline systems, *Rev. Scient. Instrum.* **56,** 291–296 (1985).
25. W. D. Bennon and F. P. Incropera, A continuum model for momentum, heat and species transport in binary solid–liquid phase change systems—II. Application to solidification in a rectangular cavity, *Int. J. Heat Mass Transfer* **30,** 2171–2187 (1987).
26. L. W. Wang and C. T. Chen, Thermosolutal convection in high-aspect-ratio enclosures, NASA Tech. Memo. 100803, Lewis Research Center, Cleveland, Ohio (1988).

SOLIDIFICATION D'UNE SOLUTION AQUEUSE DE CHLORURE D'AMMONIUM DANS UNE CAVITE RECTANGULAIRE—I. ETUDE EXPERIMENTALE

Résumé—Une étude expérimentale de la solidification a été conduite pour une solution binaire NH_4Cl–H_2O, dans une cavité rectangulaire, avec une concentration initiale variée et différentes conditions aux limites thermiques. Des écoulements conduits par la convection massique influencent fortement les vitesses de solidification, les refusions locales et la redistribution macroscopique du soluté. Le contrôle de ces écoulements peut être assuré par la sélection des conditions thermiques imposées au mécanisme de solidification.

DER ERSTARRUNGSPROZESS EINER WASSERHALTIGEN AMMONIUMCHLORIDLÖSUNG IN EINEM RECHTECKIGEN HOHLRAUM—I. EXPERIMENTELLE UNTERSUCHUNGEN

Zusammenfassung—Der Erstarrungsvorgang einer binären NH_4Cl–H_2O-Lösung in einem rechteckigen Hohlraum wird abhängig von der Anfangskonzentration und den thermischen Randbedingungen experimentell untersucht. Dabei ergibt sich, daß konzentrationsgetriebene Strömungen den Erstarrungsprozeß stark beeinflussen und zu lokalem Wiederaufschmelzen und einer veränderten makroskopischen Konzentrationsverteilung führen können. Eine Beeinflussung dieser Strömungsvorgänge kann durch die Wahl der (dem Erstarrungsvorgang) aufgeprägeten thermischen Randbedingungen erreicht werden.

ЗАТВЕРДЕВАНИЕ ВОДНОГО РАСТВОРА ХЛОРИДА АММОНИЯ В ПРЯМОУГОЛЬНОЙ ПОЛОСТИ—I. ЭКСПЕРИМЕНТ

Аннотация—Экспериментально изучено затвердевание бинарного раствора NH_4Cl–H_2O в прямоугольной полости с изменяющимися начальной концентрацией и тепловыми граничными условиями. Найдено, что возникающие при этом течения сильно влияют на скорости затвердевания, локализованное повторное плавление и макроскопическое перераспределение растворенного вещества. Управление этими потоками осуществляется посредством надлежащего выбора тепловых условий.